



Influence of transient flow and solder bump resistance on underfill process

J.W. Wan^a, W.J. Zhang^{b,*}, D.J. Bergstrom^b

^aGuangzhou University, Guangzhou, 510405, China

^bDepartment of Mechanical Engineering, University of Saskatchewan, 57 Campus Dr., Saskatoon, SK S7N 5A9, Canada

Received 24 November 2004; received in revised form 15 April 2005; accepted 1 May 2005

Abstract

The underfill flow process is one of the important steps in Microsystems technology. One of the best known examples of such a process is with the flip-chip packaging technology which has great impact on the reliability of electronic devices. For optimization of the design and process parameters or real-time feedback control, it is necessary to have a dynamic model of the process that is computationally efficient yet reasonably accurate. The development of such a model involves identifying any factors that can be neglected with negligible loss of accuracy. In this paper, we present a study of flow transient behavior and flow resistance due to the presence of an array of solder bumps in the gap. We conclude (1) that the assumption of steady flow in the modeling of the flow behavior of fluids in the flip-chip packaging technology is reasonable, and (2) the solder bump resistance to the flow can not be neglected when the clearance between any two solder bumps is less than 60–70 μm . We subsequently present a new model, which extends the one proposed by Han and Wang in 1997 by considering the solder bump resistance to the flow.

© 2005 Elsevier Ltd. All rights reserved.

Keywords: Transient effect; Solder bump resistance; Dynamic contact angle; Underfill flow; Fluid filling time

1. Introduction

In micro-fabrication and bioengineering, we deal with the underfill flow process. Typically, the gap height of the fluid flow domain is relatively small in comparison to the width. In addition, there are solder bumps in the gap, which are arranged perpendicular to the flow direction. The fluids are typically non-Newtonian or otherwise complex. For instance, in the case of the flip-chip technology in electronics packaging, the gap size is usually in the range of 35 to 100 μm , the clearance between two solder bumps is usually in the range of 50 to 250 μm , and the fluid material is epoxy. The flow is driven by an external pressure or by capillary action. Two performance indices are commonly used to assess the quality of the underfill process: the uniformity of fluid distribution and the time for the fluid to fill a gap.

Most studies [1–7] reported in the literature apply the Washburn model [8] in the case of two parallel plates as shown in Fig. 1. This results in the following model

$$x_f^2 = \frac{\sigma h \cos \theta}{3\mu} t \quad (1)$$

where σ is the surface tension coefficient, x_f is the position of the flow-front at time t , θ is the contact angle, μ is the viscosity, and h is the thickness of the cavity. From Eq. (1), the filling time t_f of encapsulation can be found by taking x_f as L , i.e.

$$t_f = \frac{3\mu L^2}{\sigma h \cos \theta} \quad (2)$$

where L is the length of the cavity.

Unfortunately, predictions using the above model do not agree with the measured results [6,7,9,10]. Han and Wang [4] extended the Washburn model by incorporating the concept of “dynamic contact angle.” The dynamic contact angle proposed by Schonhorn et al. [11] describes the change of contact angle with time, in their case for an open-flow process of polymer melts from an initial state to an equilibrium state. In the study for a capillary flow within a tube reported by Newman [12], for a horizontal capillary flow, the dynamic contact angle can be calculated by the following equation

$$\cos \theta = \cos \theta_e (1 - ae^{-ct}) \quad (3)$$

* Corresponding author.

E-mail address: wjz485@mail.usask.ca (W.J. Zhang).

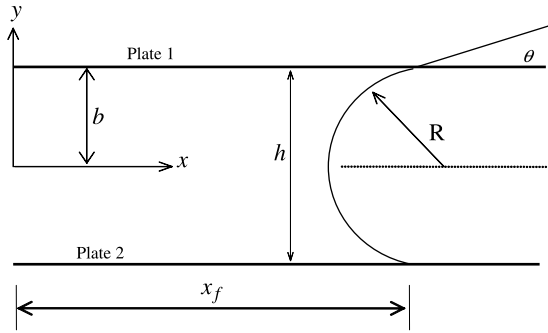


Fig. 1. Flow between two parallel plates.

where θ_e is the contact angle at an equilibrium state, a and c are coefficients, which are determined by

$$a = 1 - \frac{\cos \theta_0}{\cos \theta_e} \quad (4)$$

$$c = \frac{\sigma}{\mu M} \quad (5)$$

where θ_0 is the initial contact angle, and M is a constant which depends on the surface in contact with the encapsulant. Based on this model, i.e. Eqs. (3)–(5), Han and Wang [4] applied the dynamic contact angle model to the capillary flow between two parallel-plates and obtained

$$t_f = \frac{3\mu L^2}{\sigma h \cos \theta_e} + \frac{a}{c} (1 - e^{-ct_f}) \quad (6)$$

Eq. (6) is a nonlinear function of filling time t_f , which can be solved with an iterative scheme.

Han and Wang [4] experimentally tested their model for a flip-chip underfill flow and found that their model performed better than the Washburn model, but still did not match the experimental results. Two possible causes for this discrepancy are: (1) the transient behavior of the flow may have a significant effect on the overall behavior of the viscous flow with a free flow-front boundary; (2) the effect of the solder bump resistance on the flow may be significant. In study presented in this article, we modeled the transient flow to examine the first cause, and we extended Eq. (6) by taking into account the flow resistance due to the presence of solder bumps to examine the second cause.

2. Analysis of transient flow between two parallel plates

2.1. Model for the flow front considering the flow transient behavior

In the analysis of the flow process shown in Fig. 1, we assume: (1) the fluid is incompressible; (2) the flow is fully developed laminar flow in a two-dimensional domain, and (3) gravity is neglected. Under these assumptions, the momentum equations are simplified to be

$$\rho \frac{\partial u}{\partial t} = -\frac{\partial p}{\partial x} + \mu \frac{\partial^2 u}{\partial y^2} \quad (7)$$

$$0 = -\frac{\partial p}{\partial y} \quad (8)$$

From Eq. (8), it can be concluded that the pressure is only a function of x , i.e. $p=p(x)$. Rewriting Eq. (7) gives

$$\frac{1}{\nu} \frac{\partial u}{\partial t} = -\frac{1}{\mu} \frac{dp}{dx} + \frac{\partial^2 u}{\partial y^2} \quad (9)$$

where $\nu=\mu/\rho$ is the kinematic viscosity. For a solution domain consisting of half the channel, the initial and boundary conditions for the flow are given, respectively, by:

$$u(y, 0) = 0 \quad (10)$$

$$\frac{\partial u(0, t)}{\partial y} = 0 \quad (11)$$

$$u(b, t) = 0 \quad (12)$$

By solving the above model, i.e. Eq. (9) with the initial and boundary conditions for the flow [13], we obtain

$$\frac{u(y, t)}{(-dp/dx)b^2/\mu} = \frac{1}{2} \left[1 - \left(\frac{y}{b} \right)^2 \right] - 2 \sum_{n=0}^{\infty} \frac{(-1)^n}{(\lambda_n b)^3} \exp(-\lambda_n^2 \nu t) \cos \lambda_n y \quad (13)$$

where

$$\lambda_n b = \frac{(2n + 1)\pi}{2} \text{ and } a_n = -2 \frac{(-dp/dx)}{\mu} \frac{(-1)^n b^2}{(\lambda_n b)^3}, \quad n = 0, 1, 2, 3, \dots$$

The speed of the flow-front is equal to the mean velocity, which can be obtained by

$$u_m = \frac{1}{b} \int_0^b u dy = \left(-\frac{dp}{dx} \right) \frac{b}{\mu} \left[\frac{1}{3} b - 2 \sum_{n=0}^{\infty} \frac{(-1)^n}{(\lambda_n b)^3} \exp(-\lambda_n^2 \nu t) \frac{(-1)^n}{\lambda_n} \right]$$

or

$$u_m = \frac{dx_f}{dt} = \left(-\frac{dp}{dx} \right) \frac{b^2}{\mu} \left[\frac{1}{3} - 2 \sum_{n=0}^{\infty} \frac{1}{(\lambda_n b)^4} \exp(-\lambda_n^2 \nu t) \right] \quad (14)$$

Notice that dp/dx is assumed to be constant and can be expressed by

$$-\frac{dp}{dx} = \frac{p_0 - p_f}{x_f} = \frac{\Delta p}{x_f}$$

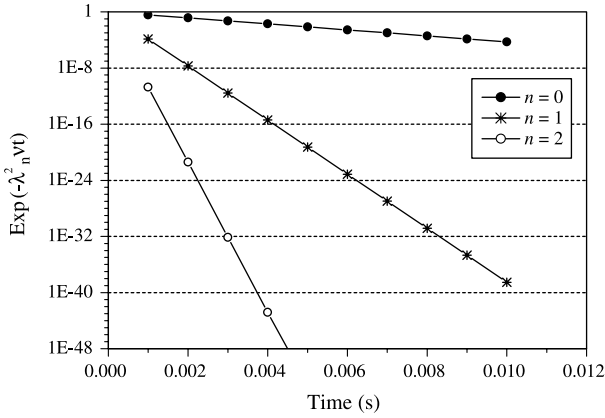


Fig. 2. Variation of $\exp(-\lambda_n^2 \nu t)$ with n (The fluid is water with a gap height of $h = 100 \mu\text{m}$).

where p_0 is the pressure at $x=0$. Substituting the above equation into Eq. (14) gives

$$\frac{dx_f}{dt} = \frac{\Delta p b^2}{x_f \mu} \left[\frac{1}{3} - 2 \sum_{n=0}^{\infty} \frac{1}{(\lambda_n b)^4 \lambda_n^2 \nu} \exp(-\lambda_n^2 \nu t) \right] \quad (15)$$

Integrating Eq. (15) and rearranging it leads to

$$x_f^2 = \frac{2 \Delta p b^2}{\mu} \left[\frac{1}{3} t - 2 \sum_{n=0}^{\infty} \frac{1}{(\lambda_n b)^4 \lambda_n^2 \nu} - 2 \sum_{n=0}^{\infty} \frac{\exp(-\lambda_n^2 \nu t)}{(\lambda_n b)^4 \lambda_n^2 \nu} \right] \quad (16)$$

2.2. Significance of the flow transient behavior

Eq. (16) consists of two time-dependent parts, the combined effect of which will be assessed in this section. First, the factor $\exp(-\lambda_n^2 \nu t)$ in the second series term is examined. The variation of $\exp(-\lambda_n^2 \nu t)$ versus time for different values of n and a gap height of $100 \mu\text{m}$ is plotted in Fig. 2. The figure shows that this term decreases very quickly with time. When $n \geq 1$, it can be seen that after 0.001 s , the term drops to a value less than 1.40×10^{-04} , which means that it is a conservatively large estimate to use only one term ($n=0$) for considering the influence of time in the factor $\exp(-\lambda_n^2 \nu t)$. That is, by including only $\lambda_0 = (\pi/2b) = (\pi/h)$, Eq. (16) becomes

$$x_f^2 = \frac{2 \Delta p b^2}{3 \mu} t - \frac{4 \Delta p b^2}{\mu} \left(1 - \exp\left(-\frac{\pi^2}{h^2} \nu t\right) \right) \sum_{n=0}^{\infty} \frac{1}{(\lambda_n b)^4} \frac{1}{\lambda_n^2 \nu} \quad (17)$$

In Eq. (17), the effect of the gap height on the term $\exp(-\pi^2 \nu t/h^2)$ with respect to time is plotted in Fig. 3. It can be seen from this figure that the term $\exp(-\pi^2 \nu t/h^2)$ also decreases very quickly with time. For a cavity thickness of $50 \mu\text{m}$, the term $\exp(-\pi^2 \nu t/h^2)$ drops to a value less than 0.019 after 0.001 s . Note that the fast-flow underfill materials used today typically take about 60 s to underfill a common-size chip ($6 \text{ mm} \times 6 \text{ mm}$) for a gap height of $50 \mu\text{m}$. Since the cavity thickness in the flip-chip package is

usually around $50 \mu\text{m}$ and the viscosities of encapsulant materials are greater than the viscosity of water, it is reasonable to drop the second term $\exp(-\pi^2 \nu t/h^2)$ in Eq. (17) for the underfill flow. Thus, Eq. (17) can be approximated as

$$x_f^2 \approx \frac{2 \Delta p b^2}{3 \mu} t - \frac{4 \Delta p b^2}{\mu} \sum_{n=0}^{\infty} \frac{1}{(\lambda_n b)^4 \lambda_n^2 \nu} \quad (18)$$

in which the second term is a conservatively high estimate based on the preceding analysis. The study of Wan [14] demonstrated that with respect to the sum in Eq. (18), the relative error introduced by only taking the first term of the series is less than 1.6% . Therefore, it is sufficient to retain only the first term of the sum; as such, Eq. (18) becomes

$$x_f^2 = \frac{h^2 \Delta p}{2 \mu} \left(\frac{1}{3} t - \frac{32 h^2}{\pi^6 \nu} \right) \quad (19)$$

The filling time can be obtained from Eq. (19) as

$$t_f = \frac{6 \mu}{h^2 \Delta p} x_f^2 + \frac{96 h^2}{\pi^6 \nu} \quad (20)$$

In the case of the underfill flow driven by capillary action between two-parallel plates, the pressure drop is balanced by surface tension, which can be calculated using the following equation [5,15]

$$\Delta p = \frac{2 \sigma \cos \theta}{h} \quad (21)$$

Substituting Eq. (21) into Eqs. (19) and (20) gives, respectively,

$$x_f^2 = \frac{h \sigma \cos \theta}{\mu} \left(\frac{1}{3} t - \frac{32 h^2}{\pi^6 \nu} \right) \quad (22)$$

$$t_f = \frac{3 \mu}{h \sigma \cos \theta} x_f^2 + \frac{96 h^2}{\pi^6 \nu} \quad (23)$$

From Eq. (23), it can be seen that the second term, which is associated with the unsteady flow process, is only related to the cavity thickness and the viscosity of the encapsulant.

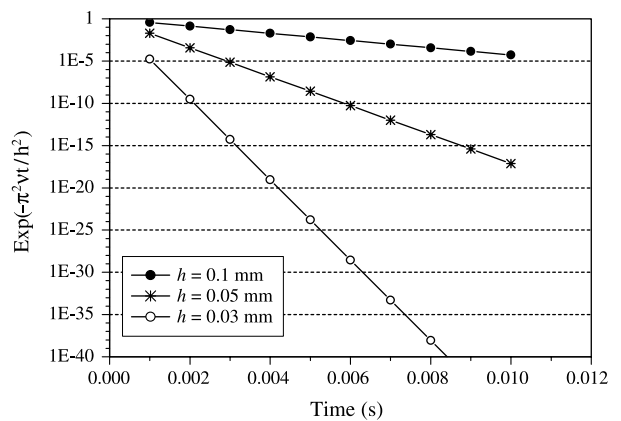


Fig. 3. Variation of $\exp(-\lambda_n^2 \nu t)$ for different gap heights (The fluid is water with $n=0$).

Table 1
 Δt_f associated with the unsteady process

Materials	μ (Pa s)	ν (m ² /s)	$\Delta t_f = 96h^2/\pi^6\nu$ (s)		
			$h = 100 \mu\text{m}$	$h = 50 \mu\text{m}$	$h = 30 \mu\text{m}$
Water	1.0×10^{-3}	1.01×10^{-6}	9.9×10^{-4}	2.50×10^{-04}	8.9×10^{-05}
SAE 30 oil	0.29	3.25×10^{-4}	3.08×10^{-06}	7.70×10^{-07}	2.77×10^{-07}
Glycerin	1.5	1.18×10^{-3}	8.49×10^{-07}	2.12×10^{-07}	7.64×10^{-08}

Let Δt_f denote the unsteady part of the filling time, i.e.

$$\Delta t_f = \frac{96h^2}{\pi^6\nu} \quad (24)$$

Table 1 lists the value of Δt_f for three different fluids (with different viscosities) and three cavity thicknesses. From the results shown in Table 1 it can be seen that Δt_f decreases with a decrease in the gap thickness and an increase in viscosity. Furthermore, the value of Δt_f is always very small. Since the gap thickness in a flip-chip package is approximately 50 μm , and the viscosities of encapsulant materials are greater than the viscosity of water, the correction term Δt_f due to the transient behavior of a flow driven by surface tension can be neglected.

To further justify the above conclusion, Table 2 lists the errors caused when only the steady part is considered for the three encapsulant materials reported by Nguyen et al. [9]. The maximum relative error is found to be 0.00014% for material C with a gap thickness of 100 μm . When the gap thickness is less than 50 μm , the maximum error is less than 0.000017%.

3. Analysis of flow resistance due to the presence of solder bumps

3.1. A model considering flow resistance due to the presence of solder bumps

The full array solder bump pattern, as a generic feature of the flip-chip package, is described in Fig. 4. The solder bump pattern can be represented by a two-row array as a representative structure (Fig. 4a). Based on the assumption that the underfill flow consists of a set of one dimensional channel flows, the problem can be further simplified to that shown in Fig. 4b. In Fig. 4, P_t is solder bump pitch, W is the clearance between two adjacent solder joints, and d is the solder diameter.

The pressure difference which drives the flow is the driving pressure Δp_σ due to surface tension reduced by the pressure loss Δp_j due to the solder bump resistance, i.e.

$$\Delta p = \Delta p_\sigma - \Delta p_j \quad (25)$$

where the surface tension component is determined by the following equation [1]

$$\Delta p_\sigma = 2\sigma \cos \theta \left(\frac{1}{W} + \frac{1}{h} \right) \quad (26)$$

where W is the width of the channel and h the thickness of the channel.

The term Δp_j in Eq. (25) is the pressure loss caused by the solder bumps. For the capillary flow shown in Fig. 4, the pressure drop, Δp_j , associated with the variation in cross-section between Sections 1 and 2, is given by [16]

$$\Delta p_j = 2\sigma \cos \theta \left[\left(\frac{1}{h_2} + \frac{1}{W} \right) - \left(\frac{1}{h_1} + \frac{1}{P_t} \right) \right] \quad (27)$$

When the channel thickness is the same, i.e. $h_1 = h_2$, the above equation reduces to

$$\Delta p_j = 2\sigma \cos \theta \left(\frac{1}{W} - \frac{1}{P_t} \right) \quad (28)$$

Table 2
 Relative error using steady model to predict filling time

Encapsulant material	A	B	C	Gap height (μm)
Viscosity (Pa-s)	0.7	0.34	0.165	
Density (kg/m ³)	1600	1600	1700	
Surface tension (N/m)	0.027	0.027	0.031	
Contact angle (degree)	25.5	20.4	17.5	
Filling time considering the unsteady term (s)	38.68272	18.09322	7.515784	100
Filling time considering the steady term only (s)	77.36544	36.18644	15.03155	50
Relative error (%)	128.9424	60.31073	25.05258	30
	38.68272	18.09322	7.515774	100
	77.36544	36.18644	15.03155	50
	128.9424	60.31072	25.05258	30
	5.9×10^{-6}	2.6×10^{-5}	1.37×10^{-4}	100
	7.38×10^{-7}	3.25×10^{-6}	1.7×10^{-5}	50
	1.6×10^{-7}	7.01×10^{-7}	3.7×10^{-6}	30

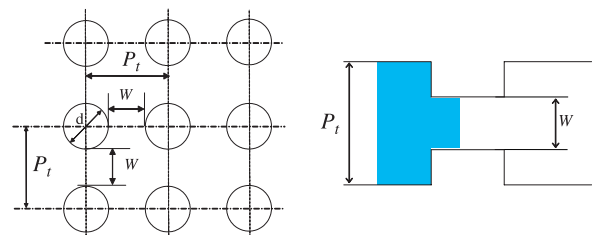


Fig. 4. Flip-chip package pattern: (a) geometry, (b) generic flow pattern.

Table 3
Constitutive constants [4]

N	K_{00} (Pa·s ⁿ)	τ_{y0} (Pa)	T_y (K)	T_g (K)	C_1	C_A	C_B (K)
0.916	153.6	0.00138	2148.6	250	3.671	18.44	199.6

Given the flip-chip geometry, an underfill flow in a flip-chip package can be approximated as a combination of a set of flow channels, as shown in Fig. 4a, for which

$$P_t = W + d \quad (29)$$

Substituting Eq. (29) into Eq. (28) gives

$$\Delta p_j = \frac{2d\sigma \cos \theta}{W(W + d)} \quad (30)$$

Substituting Eqs. (26) and (30) into Eq. (25) gives

$$\Delta p = \frac{2\sigma \cos \theta (W^2 + hW + dW - dh)}{hW(W + d)} \quad (31)$$

By substituting Eq. (31) to Eq. (15) and neglecting the transient part, we obtain

$$\frac{dx_f}{dt} = \frac{2b^2\sigma \cos \theta_e (W^2 + hW + dW - dh)}{3\mu x_f hW(W + d)} (1 - ae^{-ct}) \quad (32)$$

Integration of Eq. (32) leads to

$$x_f^2 = \frac{4b^2\sigma \cos \theta_e (W^2 + hW + dW - dh)}{3\mu hW(W + d)} \left[t + \frac{a}{c} (e^{-ct} - 1) \right] \quad (33)$$

and the filling time becomes

$$t_f = \frac{3\mu W(W + d)}{h\sigma \cos \theta_e (W^2 + hW + dW - dh)} x^2 + \frac{a}{c} (1 - e^{-ct_f}) \quad (34)$$

Since Eq. (34) is a nonlinear function of filling time t_f , an iterative procedure is needed to evaluate the equation.

3.2. Model validation

The validation of the model, i.e. Eq. (34), developed above by considering the dynamic contact angle and solder bump resistance was done using the material and constitutive model reported by Han and Wang [4]. The

Table 4
Measured and theoretical filling times

Temperature (°C)	80	50	23	23	23
Fraction of volume filled (%)	0.926	0.676	0.25	0.402	0.646
Measured filling time (s) [4]	60	180	180	600	2700
Filling time calculated with Washburn model (s) (Eq. (2))	8.58	17.6	9.84	27.35	77.47
Filling time calculated with Han-Wang model (s) (Eq. (6))	46.6	133.6	121.4	330.0	835.1
Filling time calculated with the proposed analytical model (s) (Eq. (34))	61.5	189.5	187.7	535.4	1502

material is Hysol FP4510 from Dexter Corporation USA. The viscosity of the material was measured at different temperatures, shear rates, and degrees of cure. The measured results of the material were fitted with the Herschel-Bulkley model

$$\eta = \tau_y \dot{\gamma} + K \dot{\gamma}^{n-1} \quad (35)$$

where n is the power-law index, and τ_y is the yield stress which is assumed to depend on temperature and be described by

$$\tau_y = \tau_{y0} \exp\left(\frac{T_y}{T}\right) \quad (36)$$

The coefficient K in Eq. (35) was fitted with the Williams-Landel-Ferry (WLF) equation

$$K = C_1 K_{00} \exp\left(\frac{-C_A(T - T_g)}{C_B - T - T_g}\right) \quad (37)$$

where K_{00} , C_A , C_B , T_g are constants and given in Table 3. When the thickness of cavity is different from the reference thickness $h_0 = 1.89 \times 10^{-4}$ m, the viscosity needs to be corrected using the following correlation

$$\eta = \eta_0 (4.3343 + 0.3888 \ln h) \quad (38)$$

where η_0 is the viscosity at the reference thickness h_0 . The wall shear rate is calculated by [4]

$$\dot{\gamma} = \frac{6L}{ht_f} \quad (39)$$

The equilibrium contact angle and the surface tension coefficient were fitted to the following equations, respectively,

$$\theta = 17.27 + 0.176T - 3.76 \times 10^{-4} T^2 \quad (40)$$

$$\sigma = 0.1236 \exp(-3.8 \times 10^{-3} T) \quad (41)$$

The experimental conditions reported by Han and Wang [4] are as follows: the length of the chip is 7 mm, the thickness of the cavity is 0.1 mm, the solder diameter is 0.16 mm, the clearance between adjacent solder joints is

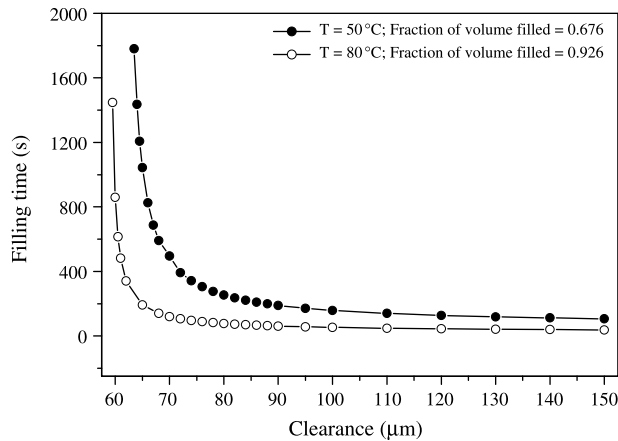


Fig. 5. Effect of the clearance on the filling time with different temperatures.

0.09 mm, the initial contact angle $\theta_0 = 84.8^\circ$, and $M = 17.1$. Under these conditions, the filling time was calculated using the proposed analytical model given by Eq. (34).

It should be noted that the underfill material of FP4510 is a non-Newtonian fluid, which means that its viscosity changes with respect to time. When applying Eq. (34) which is essentially a model for Newtonian fluid, for every time t a viscosity corresponding to t is calculated from Eq. (35), and the calculated viscosity is then substituted for the one in Eq. (34).

The filling time calculated from the new analytical model was compared with the measured filling time, as well as predictions using the Washburn and Han-Wang models (respectively), as shown in Table 4. From the results, it can be seen that the prediction using the proposed analytical model matches the measured filling times far better than the predictions using both the Washburn model and the Han-Wang model. This confirms that the flow resistance caused by the solder bump has a significant effect on the underfill flow for the specific conditions of this case. However, all the simulations are in poor agreement with the measured results at 23 °C for volume fractions of 0.402% and 0.646%. In this case, the difference between the experimental and the theoretical results may be caused by the temperature and time dependence of the viscosity. This is because the underfill flow process is to a certain degree coupled with the fluid curing process. The solidification process will affect the viscosity of the fluid, and such an effect becomes more significant with an increase in the filling time. When the underfill flow is performed at lower temperatures and longer filling times, the viscosity may increase significantly with time.

3.3. Further analysis of influences of solder bumps

Fig. 5 shows the influence of the clearance on the filling time for temperatures of 50 and 80 °C, respectively. From these results it can be seen that the filling time increases as

the clearance decreases. There appears to be a critical clearance (c_1 , approximately 100–110 μm) above which the flow resistance due to the presence of solder bumps on the filling time could be treated as a small constant. There also appears to be a second critical clearance (c_2 , approximately 60–70 μm) below which the filling time increases sharply such that the underfill process becomes impractical to implement. From Fig. 5, it can also be seen that a higher temperature tends to reduce the critical clearance c_2 , but does not affect the critical clearance c_1 .

4. Conclusions

From the results presented in this study, the following conclusions can be drawn:

- (1) For a small gap thickness (around 50 μm) and large fluid viscosity (larger than 0.1 Pa s), the influence of transient flow on the flow front and the filling time becomes negligible. Therefore, for the viscous flow process in a micro-cavity, the assumption of steady flow for the underfill process is reasonable.
- (2) The solder bump resistance has a significant effect on the underfill flow, when the clearance between solder bumps is small, e.g. less than 60–70 μm.
- (3) The proposed analytical model, i.e. Eq. (34), which further extends the Han-Wang model [4] by considering the solder bump influence, yields much better predictions than the Han-Wang model for the specific conditions of flip-chip package geometry and fluid properties reported in [4].

Acknowledgements

The authors would like to acknowledge partial financial support for this research through a NSERC discovery grant and a grant from US Intel Corp.

References

- [1] J. Wang, Underfill of flip-chip on organic substrate: viscosity, surface tension, and contact angle, *Microelectronics Reliability* 42 (2002) 293–299.
- [2] N.W. Pascarella, D.F. Balducci, Compression flow modeling of underfill encapsulation for low cost flip-chip assembly, *IEEE Transactions on Components, Packaging, and Manufacturing Technology, Part C* 21 (4) (1998) 325–335.
- [3] D.R. Gamota, C.M. Melton, Advanced encapsulant materials systems for flip-chip on board assemblies: I. Encapsulant materials with improved manufacturing properties II. Materials to integrate the reflow and underfilling processes IEEE/CPMT International electronics manufacturing technology symposium, Austin, TX, 1996 pp. 1–9.

- 673 [4] S. Han, K.K. Wang, Analysis of the flow of encapsulant during
674 underfill encapsulation of flip-chips, *IEEE Transactions on Components, Packaging, and Manufacturing Technology, Part B* 20 (4)
675 (1997) 424–433.
- 676 [5] M.K. Schwiebert, W.H. Leong, Underfill flow as viscous flow
677 between parallel plates driven by capillary action, *IEEE Transactions on Components, Packaging, and Manufacturing Technology, Part C*
678 19 (12) (1996) 133–137.
- 679 [6] G.L. Lehmann, T. Driscoll, N.R. Guydosh, P.C. Li, E.J. Cotts,
680 Underflow process for direct-chip-attachment packaging, *IEEE Transactions on Components, Packaging, and Manufacturing Technology, Part A* 21 (2) (1998) 266–274.
- 681 [7] M.H. Gordon, G. Ni, W.F. Schmidt, R.P. Selvam, A capillary-driven
682 underfill encapsulation process, *Advantaged Packaging* 8 (1999) 34–37.
- 683 [8] E.W. Washburn, The dynamics of capillary flow, *Physical Review* 17
684 (1921) 273–283.
- 685 [9] L. Nguyen, C. Quentin, P. Fine, B. Cobb, S. Bayyuk, H. Yang, S.A.
686 Bidstrup-Allen, Underfill of flip-chip on laminate: simulation and
687 validation, *IEEE Transactions on Components and Packaging Technology* 22 (2) (1999) 168–176. 729
- 688 [10] P. Fine, B. Cobb, L. Nguyen, Flip-chip underfill flow characteristics
689 and prediction, *IEEE Transactions on Components and Packaging Technology* 23 (3) (2000) 420–427. 730
- 690 [11] H. Schonhorn, H. Frisch, T.K. Kwei, Kinetics of wetting of surfaces
691 by polymer melts, *Journal of Applied Physics* 37 (1966) 4967–4973. 731
- 692 [12] S. Newman, Kinetics of wetting of surfaces by polymer: capillary
693 flow, *Journal of Colloid and Interface Science* 26 (1968) 209–213. 732
- 694 [13] V. Arpaci, *Conduction heat transfer*, Addison-Wesley Publishing
695 Company, Reading, MA, USA, 1966. 733
- 696 [14] Wan, J.W., Analysis and modeling of underfill flow driven by
697 capillary action in flip-chip packaging, PhD dissertation, University of
698 Saskatchewan, Saskatoon, SK, Canada, 2005. 734
- 699 [15] D.S. Kim, K.C. Lee, T.H. Know, Micro-channel filling flow
700 considering surface tension effect, *Journal of Micromechanics and
701 Microengineering* 12 (2002) 236–246. 735
- 702 [16] M.J. Madou, *Fundamentals of microfabrication—the science of
703 miniaturization*, CRC Press, New York, 2002. 736
- 704 737
- 705 738
- 706 739
- 707 740
- 708 741
- 709 742
- 710 743
- 711 744
- 712 745
- 713 746
- 714 747
- 715 748
- 716 749
- 717 750
- 718 751
- 719 752
- 720 753
- 721 754
- 722 755
- 723 756
- 724 757
- 725 758
- 726 759
- 727 760
- 728 761
- 762
- 763
- 764
- 765
- 766
- 767
- 768
- 769
- 770
- 771
- 772
- 773
- 774
- 775
- 776
- 777
- 778
- 779
- 780
- 781
- 782
- 783
- 784